J|A|C|S
ARTICLES
Published on Web 02/16/2002

EPR Study of Substrate Binding to the Mn(II) Active Site of the Bacterial Antibiotic Resistance Enzyme FosA: A Better Way To Examine Mn(II)

Stoyan K. Smoukov,[†] Joshua Telser,[†,‡] Bryan A. Bernat,[§] Chris L. Rife,[§] Richard N. Armstrong,*[,§] and Brian M. Hoffman*[,†]

Contribution from the Department of Chemistry, Northwestern University, Evanston, Illinois 60208-3113, and the Departments of Biochemistry and Chemistry and the Center in Molecular Toxicology, Vanderbilt University, Nashville, Tennessee 37232

Received November 6, 2001

Abstract: FosA is a manganese metalloglutathione transferase that confers resistance to the broad-spectrum antibiotic fosfomycin, (1*R*,2*S*)-epoxypropylphosphonic acid. The reaction catalyzed by FosA involves the attack by glutathione on fosfomycin to yield the product 1-(*S*-glutathionyl)-2-hydroxypropylphosphonic acid. The enzyme is a dimer of 16 kDa subunits, each of which harbors one mononuclear Mn(II) site. The coordination environment of the Mn(II) in the FosA·Mn^{2+} complex is composed of a glutamate and two histidine ligands and three water molecules. Here we report EPR spectroscopic studies on FosA, in which EPR spectra were obtained at 35 GHz and 2 K using dispersion-detection rapid-passage techniques. This approach provides an absorption envelope line shape, in contrast to the conventional (slow-passage) derivative line shape, and is a more reliable way to collect spectra from Mn(II) centers with large zero-field splitting. We obtain excellent spectra of FosA bound with substrate, substrate analogue phosphate ion, and product, whereas these states cannot be studied by X-band, slow-passage methods. Simulation of the EPR spectra shows that binding of substrate or analogue causes a profound change in the electronic parameters of the Mn(II) ion. The axial zero-field splitting changes from $|D| = 0.06$ cm^{-1} for substrate-free enzyme to 0.23 cm^{-1} for fosfomycin-bound enzyme, 0.28 (1) cm^{-1} for FosA with phosphate, and 0.27 (1) cm^{-1} with product. Such a large zero-field splitting is uncommon for Mn(II). A simple ligand field analysis of this change indicates that binding of the phosphonate/phosphate group of substrate or analogue changes the electronic energy levels of the Mn(II) 3d orbitals by several thousand cm^{-1}, indicative of a significant change in the Mn(II) coordination sphere. Comparison with related enzymes (glyoxalase I and MnSOD) suggests that the change in the coordination environment on substrate binding may correspond to loss of the glutamate ligand.

Introduction

FosA[1−5] is a manganese metalloglutathione transferase that confers resistance to the broad-spectrum antibiotic fosfomycin, (1*R*,2*S*)-epoxypropylphosphonic acid. The enzyme, which is a dimer of 16 kDa subunits,[2] catalyzes the addition of glutathione (GSH) to carbon-1 of fosfomycin to yield 1-(*S*-glutathionyl)-2-hydroxypropylphosphonic acid (GSfos), as illustrated in Scheme 1.

FosA is a member of the vicinal oxygen chelate (VOC) superfamily of metalloenzymes that includes glyoxalase I, extradiol dioxygenases, and methylmalonyl-CoA epimerase.[4] The structural hallmark of this superfamily is a mononuclear metal ion binding site composed of paired $\beta\alpha\beta\beta\beta$ motifs that provide a coordination environment with two or three open or solvent-occupied coordination sites. FosA is unique in the superfamily in being a member[5,6] of a very rare, but emerging, group of metalloenzymes that intrinsically employ a mononuclear Mn(II) ion in its catalytic site.[7−11] Further, FosA is

[†] Northwestern University.
[‡] Permanent address: Chemistry Program, Roosevelt University, Chicago, IL 60605
[§] Vanderbilt University.

(1) Abbreviations used: FosA, fosfomycin resistance protein (fosfomycin is (1*R*,2*S*)-epoxypropylphosphonic acid); CW, continuous wave; EPR, electron paramagnetic resonance; ENDOR, electron nuclear double resonance; ESEEM, electron spin−echo envelope modulation; E·Mn^{2+}·S, complex of the enzyme·Mn^{2+}·substrate, E·Mn^{2+}·GSf, complex of the enzyme·Mn^{2+}·product (GSf, 1-(*S*-glutathionyl)-2-hydroxypropylphosphonic acid); GSH, glutathione; hwhm, half-width at half-maximum; MnSOD, Mn superoxide dismutase; MW, microwave; VOC, vicinal oxygen chelate; zfs, zero-field splitting.

(2) Arca, P.; Rico, M.; Brana, A. F.; Villar, C. J.; Hardisson, C.; Suarez, J. E. *Antimicrob. Agents Chemother.* **1988**, *32*, 1552−1556.
(3) Bernat, B. A.; Laughlin, L. T.; Armstrong, R. N. *Biochemistry* **1997**, *36*, 3050−3055.
(4) Armstrong, R. N. *Biochemistry* **2000**, *39*, 13625−13632.
(5) Bernat, B. A.; Armstrong, R. N. *Biochemistry* **2001**, *40*, 12712−12718.
(6) Bernat, B. A.; Laughlin, L. T.; Armstrong, R. N. *Biochemistry* **1999**, *38*, 7462−7469.
(7) Boldt, Y. R.; Whiting, A. K.; Wagner, M. L.; Sadowsky, M. J.; Que, L., Jr.; Wackett, L. P. *Biochemistry* **1997**, *36*, 2147−2153.
(8) Wikaira, J.; Gorun, S. In *Bioinorganic Catalysis*, 2nd ed.; Reedijk, J., Bouwman, E., Eds.; Marcel Dekker: New York, 1999; pp 355−422.
(9) Requena, L.; Bornemann, S. *Biochem. J.* **1999**, *343*, 185−190.
(10) Lee, H. C.; Goroncy, A. K.; Peisach, J.; Cavada, B. S.; Grangeiro, T. B.; Ramos, M. V.; Sampaio, A. H.; Dam, T. K.; Brewer, C. F. *Biochemistry* **2000**, *39*, 2340−2346.
(11) Koyama, H. *Agric. Biol. Chem.* **1988**, *52*, 743−748.

10.1021/ja012480f CCC: $22.00

Scheme 1

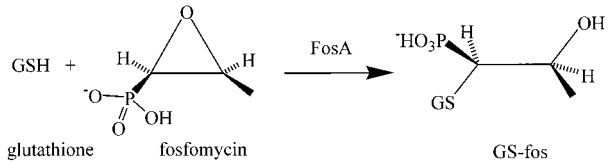

unique among the mononuclear Mn enzymes in that its catalytic activity is not coupled to a redox cycling at the Mn ion, unlike all other confirmed mononuclear manganese enzymes of which we are aware, such as manganese superoxide dismutase (MnSOD)[8,12,13] and others.[7,9]

Substantial experimental evidence with glyoxalase I, a Zn(II) enzyme, and the extradiol dioxygenases, primarily Fe(II) enzymes, suggests that the common mechanistic imperative in the VOC superfamily is a direct coordination of substrates and intermediates to the metal ion.[4] By analogy, it has been proposed that the FosA catalysis involves the coordination of fosfomycin to the Mn(II) center through displacement of one or more of the three coordinated water molecules. The resulting activation of the oxirane ring is thought to facilitate addition of the nucleophile, GSH[3,6,14] The enzymatic reaction also requires a monovalent cation (K^+) for optimum efficiency.

The mechanistic inference of direct substrate coordination to the Mn(II) of FosA has not been verified structurally or spectroscopically, and EPR in principle provides a means of addressing this question. Previous solution EPR studies employed conventional (slow-passage, absorption-mode, derivative-display) EPR spectroscopy [15] at the Q-band (35 GHz).[3] These studies showed that the enzyme itself ($E{\cdot}Mn^{2+}$) gives a readily observed $g = 2.0$ hyperfine-split sextet with $A(^{55}Mn) \approx 250$ MHz, but that addition of fosfomycin to form the substrate complex ($E{\cdot}Mn^{2+}{\cdot}S$) caused an almost complete loss of the sextet pattern, with no new signal being detected.[3] Although the loss of the sextet is consistent with the formation of the $E{\cdot}Mn^{2+}{\cdot}S$ complex with substantial change in the Mn^{2+} coordination environment, no detailed, quantitative understanding of the phenomenon can be derived from such a result.

In the present report we show that the binding of fosfomycin to FosA ($E{\cdot}Mn^{2+}$) does not abolish its EPR spectrum but alters it dramatically. We show that the signal of the $E{\cdot}Mn^{2+}{\cdot}S$ complex cannot be studied by conventional EPR spectroscopy of the unsaturated signal. However, dispersion mode detection of a saturated 35 GHz field-modulated signal at 2 K, under so-called rapid-passage conditions,[16] permits ready observation of the EPR spectrum of $E{\cdot}Mn^{2+}{\cdot}S$. This technique gives a good representation of the EPR absorption envelope, not its derivative. As a consequence, it is better suited for the study of broad peaks than are conventional techniques, which in metal centers with large zero-field splitting may give either no spectrum, as with $E{\cdot}Mn^{2+}{\cdot}S$, or an uninterpretable one. The benefit of the dispersion mode rapid-passage approach was demonstrated long ago,[17] and we hope that the present report will encourage wider use of this technique in the study of high-spin metalloenzyme systems.

The present EPR measurements permit us to determine the zero-field splitting parameters of the Mn(II) ($S = {}^5/_2$) ion not only in FosA but also in the ternary complexes with substrate fosfomycin, with inorganic phosphate, which is a substrate analogue, and with the product (GSf). A simple ligand-field analysis leads us to suggest that binding of the fosfomycin anion occurs via inner sphere coordination of phosphonate to the metal and the release of the anionic protein ligand, glutamate 113, behavior similar to that observed with the structurally characterized and related VOC enzyme, glyoxalase I. Analogies are also drawn with the coordination chemistry of MnSOD.

Materials and Methods

Protein Sample Preparation. Fosfomycin disodium salt and 4-(2-hydroxyethyl)piperazine-1-ethanesulfonic acid (HEPES) were purchased from Fluka (Ronkonkoma, NY). Glutathione was obtained from Sigma (St. Louis, MO). Tetramethylammonium (TMA) chloride and TMA hydroxide were purchased from Aldrich (Milwaukee, WI). The product, 1-(*S*-glutathionyl)-2-hydroxypropylphosphonic acid (GSf), was synthesized, purified, and converted to its tetramethylammonuim salt as previously described.[14] Apo FosA was prepared as previously described.[3]

For all 35-GHz EPR samples reported here, the FosA:Mn(II) concentration ratio was 10:1, minimizing the possibility that both mononuclear Mn(II) binding sites in dimeric FosA would be occupied, which could cause intramolecular spin−spin relaxation and could distort the EPR spectra. The following compositions were typical: 5 mM protein concentration, 0.5 mM Mn(II), pH = 8, 100 mM HEPES buffer. The samples made with K^+ ions also contained 100 mM KCl. Typical $E{\cdot}Mn^{2+}{\cdot}S$ samples in addition contained 10 mM fosfomycin, $E{\cdot}Mn^{2+}{\cdot}PO_4$ samples in addition contained 20 mM phosphate, and $E{\cdot}Mn^{2+}{\cdot}GSf$ samples in addition contained 10 mM GSf. Typical $Mn^{2+}{\cdot}S$ samples contained ~1 mM Mn(II) and ~70 mM fosfomycin in 100 mM HEPES buffer.

$[Mn(H_2O)_6]^{2+}$ Preparation. $[Mn(H_2O)_6]^{2+}$ was prepared by dissolving $Mn(OAc)_2$ in ethanol/water (1:1 v/v). Ethanol was used since it has been reported to sharpen EPR spectra better than glycerol.[18]

Mn(II)/PO_4 Preparation. Mn(II)/PO_4 was prepared by adding 10 μL of 100 mM solution of $MnSO_4{\cdot}H_2O$ to approximately 1 mL (990 μL) of phosphate buffer at pH = 5.8.

EPR Experiments and Simulations. The 35-GHz CW EPR/ENDOR spectrometer has been previously described.[19] EPR spectra were simulated with a FORTRAN computer program, DDPOWHE, that employs the full-spin Hamiltonian for a high-spin system.[20] The spin Hamiltonian is given below

$$\mathscr{H} = \sum B_k^q O_k^q \; (k \le 2S;\, q \text{ even},\, q \le k) + \beta H{\cdot}g{\cdot}S + \beta_N g_N H{\cdot}I + S{\cdot}\mathbf{A}{\cdot}I + I{\cdot}\mathbf{P}{\cdot}I \quad (1)$$

where the terms correspond to zero-field splitting (zfs, fine structure), electronic and nuclear Zeeman splitting, and hyperfine and nuclear quadrupole coupling, respectively, in approximate order of decreasing energy. The expression for the fine structure terms in eq 1 is the most general form, where O_k^q are spin operators and $B_k q$ are the corresponding energy parameters. For Mn(II) (high-spin d,[5] $S = {}^5/_2$), both second order (axial distortion, $B_2^0 O_2^0$, $D \equiv 3B_2^0$; rhombic distortion, $B_2^2 O_2^2$, $E \equiv B_2^2$) and fourth order [B_4, B_4^0 (O_4^0 with O_4^4 or O_4^3); cubic and

(12) Un, S.; Dorlet, P.; Voyard, G.; Tabares, L. C.; Cortez, N. *J. Am. Chem. Soc.* **2001**, *123*, 10123−10124.
(13) Campbell, K. A.; Yikilmaz, E.; Grant, C. V.; Gregor, W.; Miller, A.-F.; Britt, R. D. *J. Am. Chem. Soc.* **1999**, *121*, 4714−4715.
(14) Bernat, B. A.; Laughlin, L. T.; Armstrong, R. N. *J. Org. Chem.* **1998**, *63*, 3778−3780.
(15) Poole, C. P., Jr. *Electron Spin Resonance*; 2nd ed.; John Wiley & Sons: New York, 1983.
(16) Mailer, C.; Taylor, C. P. S. *Biochim. Biophys. Acta* **1973**, *322*, 195−203.
(17) Schulz, C. E.; Devaney, P. W.; Winkler, H.; Debrunner, P. G.; Doan, N.; Chiang, R.; Rutter, R.; Hager, L. P. *FEBS Lett.* **1979**, *103*, 102−105.
(18) Ross, R. T. *J. Chem. Phys.* **1965**, *42*, 3919−3922.
(19) Werst, M. M.; Davoust, C. E.; Hoffman, B. M. *J. Am. Chem. Soc.* **1991**, *113*, 1533−1538.
(20) Abragam, A.; Bleaney, B. *Electron Paramagnetic Resonance of Transition Ions*; Dover Publications: New York, 1986.

tetragonal or trigonal, respectively, $a \equiv 120B_4$, $F \equiv 180B_4^0$, and $B_4^2O_4^2$ (rhombic, $b \equiv 3B_4^2$)] zero-field splitting terms are possible. While all the terms in eq 1 can be incorporated into the Hamiltonian matrix generated by DDPOWHE, given the large number of parameters for $S = {}^5/_2$, we have not considered fourth-order zero-field splitting terms, although contributions from these effects are doubtless present. Also higher order electronic Zeeman and nuclear hyperfine terms, such as terms in $H^p \cdot S^q$ and $S^p \cdot I^q$, where $(p + q)$ is even, and $\leq 2S$, e.g., $H \cdot S$,[3,21] are possible but have not been considered.

Matrix diagonalization using EISPACK subroutines yields the eigenvalues and eigenvectors, from which the EPR transition energies and probabilities, respectively, are determined. The program contains a temperature-dependent Boltzmann weighting factor, a general line-broadening feature, and a line width parameter that depends on m_S or m_I (a fine or hyperfine "strain" parameter). The program uses the igloo grid method to calculate the powder pattern; use of igloo = 100 gave simulated spectra with a smooth powder pattern appearance over the entire field range. DDPOWHE also has the ability to select the specific transitions among the many possible in a high-spin system with hyperfine splitting (e.g., there are 630 possible transitions for an $S = {}^5/_2$, $I = {}^5/_2$ system as in ^{55}Mn(II)). In a frequency regime where the groups of peaks from different spin manifolds are not clearly separated, such a feature of the simulation program is helpful. This feature allows determination of the spin-manifold origin of peaks with varying saturation properties so that the behavior might be related to their origin. It is also helpful in advanced resonance techniques (ENDOR or ESEEM) that rely on monitoring the signal intensity of a specific transition (i.e., at a fixed magnetic field). Computations were performed on an IBM RS/6000 Model 560, running IBM AIX Version 3.2.5.0 for RISC System/6000, part of the Northwestern University Chemistry Computing Facility.

Given the common use of fluid solutions and/or absorption-derivative presentation, which do not in general give a good representation of the full EPR spectrum of a Mn(II) ($S = {}^5/_2$) ion, we recall here its principal features. For an isotopic g tensor, $\mathbf{g} = 2.00$, common for Mn(II), and zfs parameters, $4D \ll h\nu$ and $E = 0$, where ν is the microwave frequency, then the first-order powder (frozen-solution) EPR absorption spectrum shows a central peak at $g = 2$, associated with the $|S, M_S\rangle = |{}^5/_2, \times b1^1/_2\rangle$ to $|{}^5/_2, \mp{}^1/_2\rangle$ transition. In addition, the $|{}^5/_2, \pm{}^5/_2\rangle$ to $|{}^5/_2, \pm{}^3/_2\rangle$ and $|{}^5/_2, \pm{}^3/_2\rangle$ to $|{}^5/_2, \pm{}^1/_2\rangle$ ($\Delta M_S = \pm 1$) transitions each shows two features: a "step" where the external field is parallel to the zfs axis ("z"), and a peak where the external field is "perpendicular". The parallel transitions appear at $\pm 4D'$ ($D' \equiv D/g\beta$) and $\pm 2D'$, and the perpendicular at $\pm 2D'$ and $\pm D'$, respectively, for $|{}^5/_2, \pm{}^5/_2\rangle$ to $|{}^5/_2, \pm{}^3/_2\rangle$ and $|{}^5/_2, \pm{}^3/_2\rangle$ to $|{}^5/_2, \pm{}^1/_2\rangle$. The perpendicular transitions are more intense; as they also overlap the parallel transitions at $\pm 2D'$; in general only the outer parallel transition can be easily resolved.

When the "outer edges" of a spectrum are well-resolved, as is typically the case at 35 GHz when $|D| \gtrsim 0.1$ cm^{-1}, a good first approximation to D may be obtained from the total ($8D'$) breadth of this pattern, and this estimate is refined by computer simulations. In practice, at 35 GHz for $|D| \lesssim 0.10$ cm^{-1}, the edges of the higher manifold transitions may not be resolved, as in the case here for E·Mn^{2+}, but refinement of $|D|$ by simulation still is possible. For illustration, Figure S1A (Supporting Information) presents a simulated 35-GHz spectrum using $D = 0.1$ cm^{-1}, $E = 0$. When $E \neq 0$, then the perpendicular peaks each split into "x" and "y" branches,[22−24] as shown in Figure S1B. In addition, hyperfine interaction with ^{55}Mn ($I = {}^5/_2$, 100%) in principle splits each of these fine-structure features into sextets,[25,26] but this splitting is usually resolved only on the central transition.

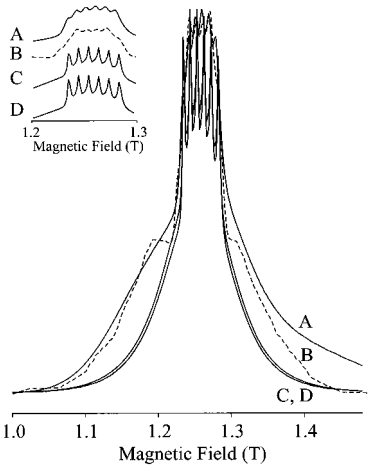

Figure 1. CW EPR of E·Mn^{2+}, Mn^{2+}·S, and Mn(II) with simulations. (A) E·Mn^{2+}: MW frequency = 35.111 GHz, 100 kHz modulation amplitude = 0.068 mT, $T = 2$ K, time constant = 64 ms, scan speed = 0.2 T/min, MW power = 20 dB, 1000 points per scan. (B) E·Mn^{2+} simulation parameters: $S = {}^5/_2$, with $D = 0.060$ cm^{-1}, $E = 0.006$ cm^{-1}, $g = 2.00$ (isotropic). (C) Mn^{2+}·S as in spectrum A, except frequency = 35.006 GHz. (D) Mn(II) as spectrum A, except MW frequency = 34.950 GHz.

Results

X-Band Derivative-Display (Slow-Passage) EPR. For comparison to 35-GHz results, we collected frozen-solution spectra of E·Mn^{2+} and E·Mn^{2+}·S at the X-band at 77, ∼50, and 4 K under the common slow-passage conditions, under which the detection of the 100-kHz field-modulated spectrum gives a derivative display. E·Mn^{2+} showed the intense sextet from the $|S, M_S\rangle = |{}^5/_2, \pm{}^1/_2\rangle$ transition at $g = 2$, along with wings on either side of this pattern whose breadth is determined by D and which in principle could be analyzed to give the zfs parameter D. We did not observe any signal from the frozen solution of E·Mn^{2+}·S at 77 or ∼50 K. At 4 K a single, broad feature was observed extending from 0 to 1000 G, as well as several weak and poorly defined features to higher field (Figure S2). This spectrum is uninterpretable; it can even be assigned to E·Mn^{2+}·S only because of the 35-GHz results to be presented.

35-GHz Rapid-Passage EPR. A series of 35-GHz EPR spectra were recorded for E·Mn^{2+}, E·Mn^{2+}·S, E·Mn^{2+}·GSf, and E·Mn^{2+}·PO$_4$ at 2 K with 100-kHz field modulation in dispersion mode under adiabatic rapid-passage conditions; these conditions yield the EPR absorption line shape, not its derivative.[16]

Figure 1 presents the 35-GHz absorption-display spectrum for E·Mn^{2+} (Figure 1A; for the simulation, see Figure 1B, below), along with those of [Mn(H$_2$O)$_6$]$^{2+}$ in the presence of the substrate antibiotic fosfomycin (Mn^{2+}·S, Figure 1C) and of [Mn(H$_2$O)$_6$]$^{2+}$ alone (Mn^{2+}, Figure 1D). Although the difference between the spectra of Mn(II) and E·Mn^{2+} is readily apparent, as seen in Figure 1, the general appearance of the spectra is similar: a sharp sextet arising from hyperfine splitting by ^{55}Mn ($I = {}^5/_2$, 100%) at $g = 2.0$, plus broad shoulders not seen in absorption-derivative spectra. The sharp peaks are associated with the $|S, M_S\rangle = |{}^5/_2, \pm{}^1/_2\rangle$ transitions and are those seen in

(21) McGavin, D. G.; Tennant, W. C.; Weil, J. A. *J. Magn. Reson.* **1990**, *87*, 92−109.
(22) Reed, G. H.; Markham, G. D. In *Biological Magnetic Resonance*; Berliner, L. J., Reuben, J., Eds.; Plenum Press: New York & London, 1984; Vol. 6, pp 73−142.
(23) Pilbrow, J. R. In *Transition Ion Electron Paramagnetic Resonance*; first ed.; Clarendon Press: Oxford, 1990; p 113.
(24) Weltner, W., Jr. In *Magnetic Atoms and Molecules*: Dover: NY, 1983; pp 266−277.
(25) Ozarowski, A.; McGarvey, B. R. *Inorg. Chem.* **1989**, *28*, 2262−2266.
(26) Doan, P. E.; McGarvey, B. R. *Inorg. Chem.* **1990**, *29*, 874−876.

conventional (derivative-display) spectra, but one sees that these do not dominate the spectrum and instead "ride on" a broader absorption associated with transitions among the other M_S of the high-spin ($S = {}^5/_2$) Mn(II) ion. The difference in appearance reflects the fact that a derivative presentation strongly discriminates against broad intense features in favor of sharp features even when, as in this case, they have low integrated intensity. The spectra of $[Mn(H_2O)_6]^{2+}$ in the presence of fosfomycin (Mn^{2+}·S, Figure 1C) and phosphate (Mn^{2+}·PO_4, not shown) are indistinguishable from the spectra of $[Mn(H_2O)_6]^{2+}$ alone (Figure 1D). This spectral identity indicates that the interaction, if any, in aqueous (glass) solution between fosfomycin (and phosphate) and free Mn(II) does not affect the electronic structure of the metal ion.[27]

There is, however, a substantial difference between the spectra of free Mn(II) (Figure 1C,D) and that of E·Mn^{2+} (FosA with a bound mononuclear Mn(II)) (Figure 1A). The characteristic Mn(II) sextet pattern, which is all that is usually detected by conventional absorption-derivative EPR spectra, is not substantially altered by incorporation into the enzyme, but the absorption display shows that the signal for E·Mn^{2+} is much broader. As described in Materials and Methods, the total spread in the field of a Mn(II) EPR spectrum is $\Delta B \equiv 8D' = 8D/g\beta$ (see Figure S1), for $4D < h\nu$,[23,24]and an approximation to $|D|$ that could be obtained by computer simulations is $|D| = 0.06 \pm 0.02$ cm^{-1}.[28,29]

The breadth of the spectrum is quite insensitive to the value of E. However, resolved hyperfine splittings were generated throughout the spectrum in simulations where $E = 0$, whereas the experimental spectrum shows hyperfine resolution only at $g = 2$. We found that the above value of $|D|$, $E = 0.006$ cm^{-1} ($E/D = 0.1$), with a constant Gaussian line width (400 MHz, hwhh), was reasonably effective in reproducing the smooth shoulders of the experimental E·Mn^{2+} EPR spectrum.[30] The simulation yields an isotropic ^{55}Mn hyperfine coupling of 250 MHz, in good agreement with the earlier report.[3] The EPR parameters for E·Mn^{2+} and the other species investigated in this report are summarized in Table 1. We note that the values for $[Mn(H_2O)_6]^{2+}$ are in excellent agreement with those in the recent, comprehensive study by Tan et al.[31,32]

Conventional EPR spectra show that substrate binding to FosA causes a loss of the Mn(II) EPR signal, but the rapid-passage technique instead shows that the spectrum of E·Mn^{2+}·S (Figure 2) is dramatically changed from that of E·Mn^{2+}. While the central sextet at $g = 2.0$ has indeed disappeared, there are EPR transitions over almost the full field range available to our

Table 1. Magnitudes for Electronic Parameters for Mn(II) in FosA and Related Species[a]

compound	$\|D\|$ (cm^{-1})	$\|E\|$ (cm^{-1})
$[Mn(H_2O)_6]^{2+}$, Mn^{2+}·S[b]	0.03(1)	negligible
E·Mn^{2+} [b]	0.06(2)	0.006(2)
E·Mn^{2+}·S	0.23(1)	0.02(1)
E·Mn^{2+}·PO_4	0.28(1)	0.02(1)
E·Mn^{2+}·GSf	0.27(1)	0.03(1)
MnSOD-azide[c]	0.046	0.009
MnSOD[c]	0.344	0.030

[a] The values for FosA and related model species were determined by computer simulation of 35-GHz EPR spectra as described in the text. An isotropic $g = 2.00$ was employed in all cases. [b] Resolved hyperfine coupling from a single ^{55}Mn was observed with isotropic $A = -250$ MHz (the sign of A is based on other studies[58−60]). [c] The values for *E. coli* MnSOD were determined by Un et al.[12] using 285- and 190-GHz EPR spectra. An isotropic $g = 2.0010$ was employed. MnSOD corresponds to the native enzyme, with five-coordinate Mn(II),[53] and MnSOD-azide corresponds to enzyme in the presence of 0.1 M azide ion. Similar parameters were obtained for Mn-reconstituted SOD from *Rhodobacter capsulatus*.

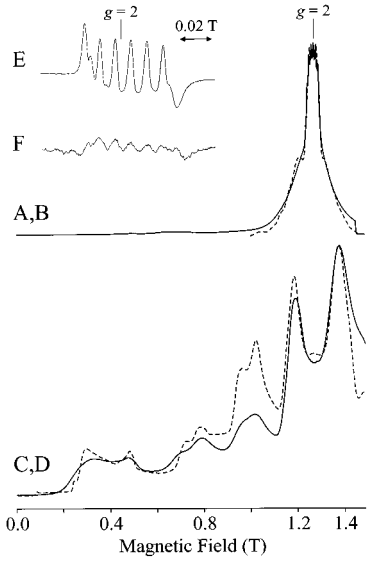

Figure 2. CW EPR of E·Mn^{2+} and E·Mn^{2+}·S. (A) E·Mn^{2+} MW frequency = 35.240 GHz, 100 kHz modulation amplitude = 0.17 mT, $T = 2$ K, time constant = 64 ms, scan speed = 0.2 T/min, MW power = 20 dB, 1000 points per scan. The sharp drop in signal at ~1.45 T is due to the magnet being shut off. (B) E·Mn^{2+} simulation parameters: $D = 0.060$ cm^{-1}, $E = 0.06$ cm^{-1}. (C) E·Mn^{2+}·S as in spectrum A, except MW frequency = 35.130 GHz, modulation amplitude = 0.068 mT. (D) E·Mn^{2+}·S simulation parameters: $D = 0.23$ cm^{-1}, $E = 0.020$ cm^{-1}. (Inset) Derivative mode CW EPR near $g = 2.0$ of (E) E·Mn^{2+} and (F) E·Mn^{2+}·S from Bernat et al.[3]

(27) It is possible that fosfomycin (phosphate) does coordinate to Mn(II) by displacement of aqua ligand(s); however, the O_6 donor set and coordination geometry is maintained so that the zfs parameters remain unchanged.

(28) The features at the extreme edges of the spectrum have very low intensity, so the apparent breadth of the "single" broad peak spectrum as measured by hwhh is much less than $8|D|/g\beta$. But since the simulations reproduce the relative intensities of those transitions as well, an overall match of the breadth between an experiment and a simulation suffices for this estimate.

(29) The central sextet saturates differently than do other transitions (Figure S3), and thus, the apparent width of the pattern varies with power, which contributes to the reported uncertainty in $|D|$.

(30) We realize that both D and E are likely distributed, which would also smooth the resolved structure resulting from a single axial zero-field splitting. As previously discussed by Kliava and Purans (Kliava, J.; Purans, J. *J. Magn. Reson.* **1980**, *40*, 33−45), the expressions for the energies of these outer fine structure transitions ($\pm{}^5/_2$ to $\pm{}^3/_2$, etc.) contain terms in D and E that vanish for the central fine structure transition ($\pm{}^1/_2$ to $\mp{}^1/_2$), so that in glasses, distributions in D and E completely broaden the outer transition lines, without broadening the central fine structure transition. As mentioned above, there are also fourth-order zfs operators, a (cubic), F (axial), and b (rhombic), all of which could be nonzero and distributed as well. These cannot be determined without single crystal studies and are likely to be small ($a < 100$ MHz),[20] but may contribute to broadening away from the central transition.

(31) Tan, X. L.; Bernardo, M.; Thomann, H.; Scholes, C. P. *J. Chem. Phys.* **1993**, *98*, 5147−5157.

(32) In this study,[31] an asymmetric skewing on the low field side of the spectrum was further taken as indicative of a negative sign of D, based on a first-order analysis of the frozen-solution spectrum and assumption of g values. However, unless the **g** tensor components are known to very high precision, such as might be possible in single-crystal studies, then the asymmetric effects of even small g anisotropy would easily outweigh effects of the sign of D (see: Bleaney, B.; Ingram, D. J. E. *Proc. R. Soc.* **1951**, *A205*, 336−356, and Ozarowski and McGarvey[25]); therefore, this assignment is not highly robust. In cases where the hyperfine splittings on $\pm{}^1/_2$ to $\mp{}^1/_2$ transition are very well-resolved, it is possible to determine the sign of the zfs parameters from second-order hyperfine shifts, but such precision is rarely available for frozen solutions (and certainly not in this case). The only general method of determining the sign of D is through the temperature-dependent changes in the anisotropy of the spectra. In the majority of Mn(II) compounds where the sign of D was determined by Bleaney and Ingram, it was negative, but there are cases where a positive sign of D was reliably determined.

magnet (0−1.5 T) (Figure 2C), and the spectrum clearly goes on to higher field.

For the E·Mn^{2+}·S spectrum (Figure 2C), we assigned the lowest field spectral feature, at a field of roughly 0.2 T (at 35 GHz), to the $|S, M_S\rangle = |^5/_2, \pm^5/_2\rangle$ to $|S, M_S\rangle = |^5/_2, \pm^3/_2\rangle$ "parallel" transition, which comes in first order at $B \approx B_0 - 4D'$ for $h\nu > 4D$,[23,24] where B_0 corresponds to $g = 2.00$ and $D' \equiv D/g\beta$; this afforded an initial estimate of $D \approx 0.2$ cm^{-1}. Ideally, we would have used the corresponding high-field transition as well, but this should come at $B \approx B_0 + 4D' \approx 2.5$ T, which is out of range for our magnet. We assumed, as was the case with E·Mn^{2+}, an isotropic $g = 2.00$. Given that no ^{55}Mn hyperfine splitting was resolved, we employed a single Gaussian line width (400 MHz, hwhh), which reproduced the experimental features. Varying D and further allowing for a rhombic zfs ($E \neq 0$) yielded a very good match between experimental and simulated spectrum with the parameters $|D| = 0.23(1)$ cm^{-1}, $|E| = 0.02(1)$ cm^{-1} (Figure 2D; Table 1.).[33] Interestingly, the computations associated with the simulation of the 35-GHz rapid-passage EPR spectra quite clearly indicated that the X-band spectra, even if all transitions were detectable (which they were not), could *not* be analyzed (See Figure S4).

We noted above that the EPR spectrum of E·Mn^{2+} shows a complicating feature whose appearance is rarely considered as dependent on microwave power (Figure S3), and the effect is even more clearly demonstrated in the EPR of E·Mn^{2+}·S (Figure S5). While this phenomenon could be a source of confusion, in fact our simulation procedures nonetheless were adequate to complete the analysis.[34]

We also investigated the ternary complex with bound phosphate, E·Mn^{2+}·PO_4 (Mn:PO_4 = 1:40), and bound product, E·Mn^{2+}·GSf (Mn:GSf = 1:20), where GSf is the product of enzyme catalysis, 1-(*S*-glutathionyl)-2-hydroxypropylphosphonic acid. The 35-GHz EPR spectrum of E·Mn^{2+}·PO_4 (Figure 3C), shows a distinct peak at $g = 2.00$ (1.25 T), while the remainder of the spectrum strongly resembles that of E·Mn^{2+}·S. The peak at $g = 2.00$ arises from residual E·Mn^{2+}, whose presence reflects a lower binding constant for phosphate than for fosfomycin (substrate). This is supported by the inset to Figure 3, which shows an expansion of the $g = 2.00$ region in which resolved hyperfine splitting is seen, just as for E·Mn^{2+}, but in contrast to E·Mn^{2+}·S. We were able to simulate the spectrum of E·Mn^{2+}·PO_4, as shown in Figure 3D, by ignoring the $g = 2$ peak, despite an even more pronounced variation in saturation behavior across this EPR spectrum (Figure S6) than for E·Mn^{2+}·S (Figure S5). The zero-field parameters are $|D| = 0.28(1)$ cm^{-1} and $E = 0.02(1)$ cm^{-1}. The relative amounts of E·Mn^{2+} and E·Mn^{2+}·PO_4 could not be quantitated reliably, however.

The analysis of the spectrum for E·Mn^{2+}·PO_4 (Figure 3C) highlights the ability of rapid-passage, absorption line shape EPR to characterize overlapping spectra with narrow, sharp features (from E·Mn^{2+}) and with broad features and a wide field spread (from E·Mn^{2+}·PO_4). Though derivative-mode EPR would have easily detected the E·Mn^{2+} component of this spectrum, the broad peaks would have been barely, if at all, distinguishable from the baseline, especially if the sextet peaks were sharp and thus the contrast even higher.

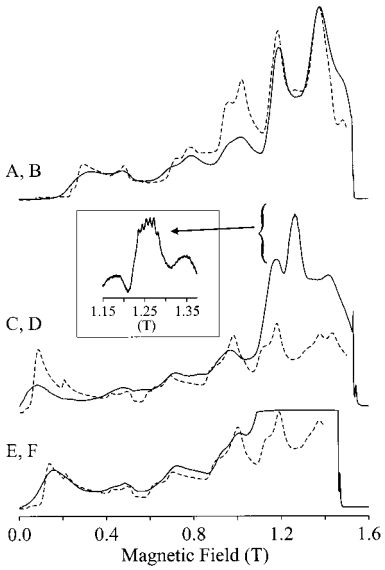

Figure 3. CW EPR of E·Mn^{2+}·S, E·Mn^{2+}·PO_4, and E·Mn^{2+}·GSf with simulations. (A) E·Mn^{2+}·S MW frequency = 35.130 GHz, 100 kHz modulation amplitude = 0.068 mT, T = 2 K, time constant = 64 ms, scan speed = 0.2 T/min, MW power = 20 dB, 1000 points per scan. The sharp drop in signal at ~1.45 T is due to the magnet being shut off. (B) E·Mn^{2+} simulation parameters: $D = 0.23$ cm^{-1}, $E = 0.020$ cm^{-1}. (C) E·Mn^{2+}·PO_4 as in spectrum A, except MW frequency = 35.124 GHz. (D) E·Mn^{2+}·PO_4 simulation parameters: $D = 0.28$ cm^{-1}, $E = 0.020$ cm^{-1}. (E) E·Mn^{2+}·GSf as in spectrum A, except MW frequency = 35.302 GHz, modulation amplitude = 0.17 mT. (F) E·Mn^{2+}·GSf simulation parameters: $D = 0.27$ cm^{-1}, $E = 0.03$ cm^{-1}. (Inset) E·Mn^{2+}·PO_4 as in spectrum A, except MW frequency = 35.124 GHz, MW power = 50 dB, scan speed = 0.125 T/min.

The low-field portion of the EPR spectrum of E·Mn^{2+}·GSf is shown in Figure 3E. As for E·Mn^{2+}·PO_4, the spectrum contains the $g = 2$ signal from E·Mn^{2+}, but in even higher proportion. This indicates that the binding of GS-fosfomycin (the product) to FosA is weaker than that of fosfomycin (substrate) and of phosphate (inhibitor). The features assigned to E·Mn^{2+}·GSf were simulated with parameters similar to those for E·Mn^{2+}·PO_4, $|D| = 0.27$ cm^{-1} and $E = 0.03$ cm^{-1} (Figure 3E). Thus, the Mn(II) ions in these three ternary complexes have highly similar coordination spheres, and these are distinctly different from that of E·Mn^{2+} (see Table 1).

Discussion

In this report, we have characterized the EPR spectra of FosA, E·Mn^{2+}, and the ternary complexes with substrate (fosfomycin), inhibitor (PO_4), and product (GSf). The EPR spectrum of E·Mn^{2+} is qualitatively the same as that for $[Mn(H_2O)_6]^{2+}$, in the resolved sextet region, but the overall breadth of the pattern is larger, which shows that the axial zfs parameter, D, is larger for E·Mn^{2+}.

In our previous report on FosA,[3] the binding of fosfomycin to FosA was characterized by the *loss* of the hyperfine-split, derivative-display EPR signal seen for E·Mn^{2+} in fluid solution in the narrow range around $g = 2.0$ and by the dramatic decrease of the ^{1}H NMR paramagnetic relaxation rate ($1/T_{1p}$) of solvent

(33) Population-based intensity weighting was not employed; the intensity match is acceptable without this additional parameter.

(34) Using a modified version of the DDPOWHE program, we were able to identify the major contributor to this peak as a $|S, M_S\rangle = |^5/_2, \pm^5/_2\rangle$ to $|^5/_2, +^3/_2\rangle$ perpendicular transition. These M_S values are actually not good quantum numbers at ~0.49 T but are appropriate at low-field (<0.1 T), where the states are well-described by $|S, M_S\rangle = |^5/_2, \pm^5/_2\rangle$, $|^5/_2, \pm^3/_2\rangle$, $|^5/_2, \pm^1/_2\rangle$, in order of ascending energy for negative D. Alternatively, using the state description appropriate at high field (>1 T) where M_S values are again good quantum numbers, this peak can be ascribed to a $|^5/_2, -^5/_2\rangle$ to $|^5/_2, +^1/_2\rangle$ perpendicular transition, which is forbidden at high field.

water, which is best explained by a decrease in the number of inner-sphere water ligands to Mn(II) in the presence of fosfomycin.

The disappearance of the E·Mn^{2+} EPR signal in fluid solution and, as we now have shown, in frozen-solution slow-passage derivative-display at the X-band as well is a negative result with several possible origins, including oxidation of Mn(II) ($S = {}^5/_2$) to Mn(III) ($S = 2$), which is EPR-invisible at conventional microwave frequencies.[13,35] Indeed, although we did *not* adopt this interpretation, the Mn(II) to Mn(III) oxidation is catalytically important for some enzymes (in MnSOD and Mn peroxidases, for example) and is favored under certain conditions.[8] We now have shown that the signal is not "lost" but that a large increase in the zero-field splitting parameters (Table 1) of the active-site high-spin Mn(II) in the ternary complexes makes the EPR signal unobservable with conventional detection methods at the X-band.

In many mononuclear Mn(II) systems, including E·Mn^{2+}, D is small (<0.08 cm^{-1}) and can be determined through analysis of conventional frozen-solution spectra taken at the X-band. If D is small and the resolution is unusually good,[25,26,36] then second-order features in the central ^{55}Mn $|S, M_S\rangle = |{}^5/_2, \pm{}^1/_2\rangle$ sextet also can be analyzed[37,38] to give D. However, as seen here for E·Mn^{2+}·S, rapid-passage dispersion detection at 35 GHz is a highly robust way to determine D, E, even when D is sufficiently large that slow-passage X-band spectroscopy fails. Rapid-passage spectroscopy at 35 GHz is particularly useful for Mn(II) centers, which typically have $D \lesssim 0.3$ cm^{-1} ($4D \lesssim h\nu$) and thus give spectra that approach the first-order limit. In principle, of course, higher frequencies than 35 GHz can be used as well. However, a very recent high-frequency EPR study (190, 285 GHz) of MnSOD that employed derivative display[12] showed only the central ^{55}Mn $|S, M_S\rangle = |{}^5/_2, \pm{}^1/_2\rangle$ transitions, and the zfs parameters could only be determined by simulation of "second-order splitting" of these features, and not by direct measurement of the outer transitions. Multiple, very high microwave frequencies in combination with a large sweep range (e.g., 0−15 T[35,39,40]) is required for integer-spin systems, such as Mn(III),[35,40] and for the few Mn(II) systems where the zero-field splittings are extremely large ($D \sim 1$ cm^{-1}).[41,42]

Implications for FosA Coordination Chemistry. The axial zero-field splitting, D, is roughly 4 times larger for the E·Mn^{2+}·S ternary complexes than for E·Mn^{2+}, for which D in turn is 2−3 times larger than for aqueous Mn(II) (Table 1). Such changes imply significant changes in its coordination sphere. For comparison, the square-planar complex MnTPP, representing the extreme case of axial distortion, has $D = -0.77$ cm^{-1}.[43] Thus, qualitatively, E·Mn^{2+}·S can be thought of as approaching a midpoint between cubic, six-coordinate $[Mn(H_2O)_6]^{2+}$ and square-planar, four-coordinate MnTPP.

To correlate the differences in zfs parameters with differences in the Mn(II) coordination sphere, we need to consider the origin of the zfs of the Mn(II) ion, a perplexing problem by itself. The free-ion ground state of Mn(II) (high-spin $3d^5$), like that of Fe^{3+}, is a $^6S_{5/2}$ state possessing zero orbital angular momentum. Thus, in the first order there is no effect of spin−orbit coupling, and $D = E = 0$. Various mechanisms have been invoked to explain the nonzero zfs observed for Mn(II). We use here the simple model commonly applied to Fe^{3+}, which incorporates spin−orbit admixing the $^6S_{5/2}$ state with a quartet ($S = {}^3/_2$) excited state and gives convenient relations between the zfs parameters and the electronic levels of the Mn(II) ion,[44−47]

$$D = (1/10)\zeta^2\,(2/E_z - 1/E_x - 1/E_y) \qquad (2a)$$

$$E = (1/10)\zeta^2\,(1/E_x - 1/E_y) \qquad (2b)$$

where ζ is the one-electron spin−orbit coupling constant and E_x, E_y, E_z are the energies for excited states that involve electron pairing of the electron in the $d_{x^2-y^2}$ orbital of the ground ($S = {}^5/_2$) state into the d_{yz}, d_{xz}, and d_{xy} orbitals, respectively. The derivation of these well-known equations, first reported by Griffith,[44,45] has never been reported to our knowledge and is given in the Supporting Information.

The zfs parameters can thus be used to calculate orbital splittings introduced by a low-symmetry coordination environment. A tetragonal distortion from the cubic symmetry of the Mn(II) ligand field causes an orbital splitting, $\Delta = E_z - (E_x + E_y)/2 \neq 0$ (a trigonal distortion would have the same effect), which introduces a nonzero value for D, while a rhombic distortion causes a further splitting, $\delta = E_x - E_y \neq 0$, and introduces a nonzero E. As we show in the Supporting Information, with quite plausible assumptions, it is possible to derive values for Δ and δ from the experimentally determined values of D and E. We shall consider models for the coordination of Mn(II) in FosA in light of the orbital splittings so derived.

The coordination sphere of the Mn(II) in E·Mn^{2+} can be inferred from the primary sequence of FosA, coupled with homology comparisons to functionally similar enzymes and the results of previous EPR studies. As shown in Figure 4, the proposed protein ligands to Mn(II) are the three nitrogen/oxygen donors, His-7, His-67, and Glu-113, as well as three solvent water molecules.[6] The specific stereochemistry at Mn(II) is hypothetical, e.g., the aqua ligands could be *mer* rather than *fac* as shown. The zfs parameters for $[Mn(H_2O)_6]^{2+}$ and E·Mn^{2+} (Table 1) give $\Delta \approx 500$ and 1000 cm^{-1}, respectively. This difference is a measure of the distortion from cubic symmetry upon replacement of three aqua ligands by the three protein residue ligands.

Formation of the ternary complex with fosfomycin, phosphate, or phosphonate causes a sharp increase in the zfs parameters (Table 1). These correspond to an increase in the tetragonal splitting from $\Delta \sim 1000$ cm^{-1} to $\Delta \sim 3800$−4700 cm^{-1} (see Supporting Information) and in the rhombic splitting, δ, from less than 200 cm^{-1} to more than 600 cm^{-1} (eqs 2a,b and

(35) Krzystek, J.; Telser, J.; Pardi, L. A.; Goldberg, D. P.; Hoffman, B. M.; Brunel, L.-C. *Inorg. Chem.* **1999**, *38*, 6121−6129.
(36) Buchbinder, J. L.; Reed, G. H. *Biochemistry* **1990**, *29*, 1799−1806.
(37) Allen, B. T. *J. Chem. Phys.* **1965**, *43*, 3820−3826.
(38) Misra, S. K. *Physica B* **1994**, *203*, 193−200.
(39) Hassan, A. K.; Pardi, L. A.; Krzystek, J.; Sienkiewicz, A.; Goy, P.; Rohrer, M.; Brunel, L. C. *J. Magn. Reson.* **2000**, *142*, 300−312.
(40) Krzystek, J.; Telser, J.; Hoffman, B. M.; Brunel, L.-C.; Licoccia, S. *J. Am. Chem. Soc.* **2001**, *123*, 7890−7897.
(41) Lynch, W. B.; Bourse, R. S.; Freed, J. H. *J. Am. Chem. Soc.* **1993**, *115*, 10909−10915.
(42) Wood, R. M.; Stucker, D. M.; Jones, L. M.; Lynch, W. B.; Misra, S. K.; Freed, J. H. *Inorg. Chem.* **1999**, *38*, 5384−5388.
(43) Hori, H.; Ikeda-Saito, M.; Reed, G. H.; Yonetani, T. *J. Magn. Res.* **1984**, *58*, 177−185.
(44) Griffith, J. S. *Biopolym. Symp.* **1964**, *No. 1*, 35−44, discussion 45−36.
(45) Griffith, J. S. *Mol. Phys.* **1964**, *8*, 213−217.
(46) Kotani, M. *Adv. Quantum Chem.* **1968**, *4*, 227−266.
(47) Pilbrow, J. R. *Transition Ion Electron Paramagnetic Resonance*; Clarendon Press: Oxford, 1990.

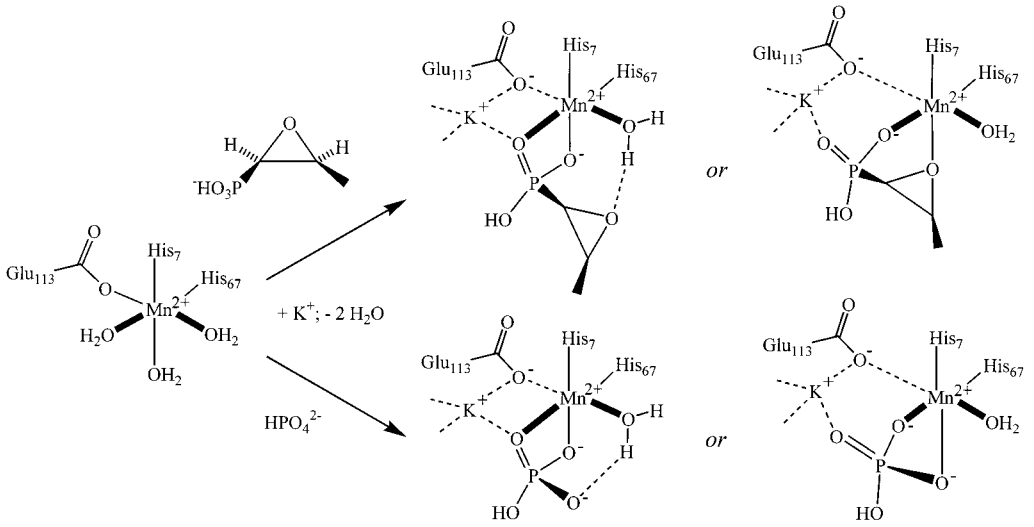

Figure 4. Possible coordination geometries for the active site in FosA with binding of substrate (fosfomycin) or analogue (phosphate) as originally proposed by Bernat et al.[6] and modified by the present results. The exact structural details remain to be elucidated. For example, in E·Mn^{2+} it is not known which nitrogen (N-δ or -ϵ) of His-7 and His-67 is bound, or whether the geometry around Mn(II) is *mer* rather than *fac*. Similarly, in E·Mn^{2+}·S and E·Mn^{2+}·PO_4, only two of several possible coordination modes for phosphonate/phosphate are shown, and the degree of protonation is uncertain. The EPR results and K^+ activation suggest that Glu-113 may move away from the coordination sphere of the metal ion upon substrate binding.

Supporting Information). Large changes in *D*, corresponding to large changes in orbital splittings, can occur upon changing the *type* of ligating atom (e.g., Cl^- to I^-).[41,42] However, the magnitude of the changes upon formation of ternary FosA complexes is striking, because in the proposed mechanisms,[3,6] the ligand donor atoms of the ternary complex do *not* change either in number or in kind (nitrogen and oxygen). Thus, in the proposed structure of the ternary complex (Figure 4), fosfomycin replaces two of the solvent water molecules with O donor ligands of its own, either via bidentate phosphonato coordination or via unidentate phosphonato with the oxirane O also acting as a ligand (see Figure 4). In either case, the coordination of both histidine nitrogen ligands is maintained.[3,6]

Moreover, one cannot propose that the large change in zfs parameters should be attributed to altered ligand field contributions from the oxygens of these reactant/inhibitor/product species, as opposed to the aqua ligands they replace, because the EPR spectra obtained for mononuclear Mn(II) with phosphato ligands in nucleic acid species, such as ribozymes, do not exhibit such large zfs constants.[48−50]

Instead, we suggest that *D* and *E* increase dramatically because the formation of the ternary complex involves a change in coordination *number*: binding of fosfomycin not only replaces the two water molecules trans to the histidine ligands, but in addition, Glu-113 is lost as a metal ion ligand in the ternary complex.[51] The loss of Glu-113 from the inner coordination sphere helps preserve the charge balance at the metal center. The formal charge at the metal center is +1 in E·Mn^{2+} and either +1 or 0 in the E·Mn^{2+}·S complex, depending on whether the second phosphonyl OH is ionized (Figure 4). The neutralization of the negative charge borne by the substrate is a key mechanistic feature of the efficient addition of an anionic nucleophile (glutathione thiolate). Thus, a formal charge of +1 in the E·Mn^{2+}·S complex would lead to a charge-neutral transition state for the addition of the nucleophile.

In support of this proposal, similar behavior is observed when the Zn^{2+} of glyoxalase I (another member of the VOC superfamily) binds a transition state analogue.[4] The Zn^{2+} ion initially is in an octahedral coordination environment, with one histidine, one glutamine, two glutamates, and two water molecules as ligands. X-ray diffraction shows that bidentate chelation of the transition state analogue replaces the two water molecules *and* that one of the glutamates leaves the inner coordination sphere,[52] with the coordination environment changing from octahedral to square pyramidal.

Further support for this proposal can be found by consideration of recent spectroscopic and crystallographic work on MnSOD.[12,53,54] In this enzyme, the Mn ion is initially in a distorted trigonal bipyramidal geometry comprising as ligands three histidines, one asparate, and one hydroxide.[53] A very recent high-field EPR study[12] has shown that *Escherichia coli* MnSOD contains Mn(II) with $|D| = 0.344$ cm^{-1}, $|E| = 0.0295$ cm^{-1}, values which are comparable to those found for E·Mn^{2+}·S (see Table 1). Addition of azide ion converts the five-coordinate Mn(II) to a six coordinate, distorted octahedral complex,[55] for which the zfs parameters are significantly smaller, $|D| = 0.0462$ cm^{-1}, $|E| = 0.0091$ cm^{-1},[12] and indeed closely resemble those for E·Mn^{2+} (see **Table 1**).

Thus the comparison among FosA, glyoxalase I, and MnSOD, suggests that, in these enzymes with histidine nitrogen and various oxygen donor ligands, a five-coordinate metal ion

(48) Morrissey, S. R.; Horton, T. E.; DeRose, V. J. *J. Am. Chem. Soc.* **2000**, *122*, 3473−3481.
(49) Manikandan, P.; Carmieli, R.; Shane, T.; Kalb, A. J.; Goldfarb, D. *J. Am. Chem. Soc.* **2000**, *122*, 3488−3494.
(50) Tan, X.; Poyner, R.; Reed, G. H.; Scholes, C. P. *Biochemistry* **1993**, *32*, 7799−7810.
(51) The proposal that substrate (fosfomycin) binding involves a ligand loss suggests that the Mn(II) ion in the fosfomycin complex has an axially elongated "crystal field", which would lead to a negative sign of *D* for the fosfomycin complex. The Supporting Information gives the derivation of the sign of *D* and its significance in terms of a simple ligand-field model, relating the spectroscopic information to molecular structure.
(52) Cameron, A. D.; Ridderstroem, M.; Olin, B.; Kavarana, M. J.; Creighton, D. J.; Mannervik, B. *Biochemistry* **1999**, *38*, 13480−13490.
(53) Edwards, R. A.; Baker, H. M.; Whittaker, M. M.; Whittaker, J. W.; Jameson, G. B.; Baker, E. N. *JBIC, J. Biol. Inorg. Chem.* **1998**, *3*, 161−171.
(54) Borgstahl, G. E. O.; Pokross, M.; Chehab, R.; Sekher, A.; Snell, E. H. *J. Mol. Biol.* **2000**, *296*, 951−959.
(55) Whittaker, M. M.; Whittaker, J. W. *Biochemistry* **1996**, *35*, 6762−6770.

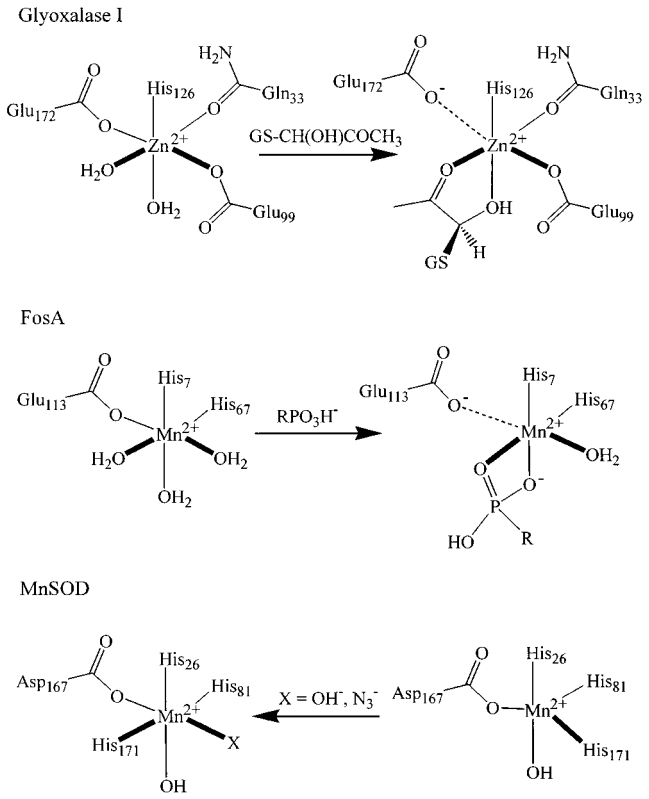

Figure 5. Comparison among the active sites of FosA, glyoxalase I, and MnSOD showing the conversion between six- and five-coordinate forms as a consequence of exogenous ligand (substrate, inhibitor) binding. The structures of FosA are proposed as described in Figure 4, and those for glyoxalase I are based on crystal structures of enzyme with transition state analogues.[52] The structure for five-coordinate MnSOD is based on X-ray crystallography of the native enzyme from *E. coli*,[53] while that for the six-coordinate form is based on that of a cryo-trapped intermediate, where X = OH^-;[54] HFEPR results described in the text are for X = N_3^-,[12] presumably with the same geometry.

complex, whether square-pyramidal or trigonal-bipyramidal, exhibits for Mn(II) $D \approx 0.3(1)$ cm^{-1}, while a six-coordinate complex has $D \approx 0.05(1)$ cm^{-1}. Figure 5 depicts the structural changes proposed for each of these three enzymes, so that the common motif can be easily seen.

In this context we recall that the reaction catalyzed by FosA depends in a so-far unexplained way on K^+ ions for optimal activity.[56] However, the E113Q mutant enzyme is almost as active as the native enzyme is in the presence of K^+, but the mutant is not activated by this monovalent cation.[6] Thus, we suggest that in the native enzyme, K^+ neutralizes the charge on the carboxylate of Glu-113, when it is lost from the coordination sphere of Mn(II) upon fosfomycin binding, as illustrated in Figure 4.

(56) Addition of an excess of K^+ ion has no observable effect on the 35-GHz EPR spectrum of E·Mn^{2+}·S (Figure S7). Thus the interaction between Glu-113 and K^+ ion does not directly affect the ground-state zfs parameters of the Mn^{2+} ion itself. Addition of K^+ ion to E·Mn^{2+}·S had been previously shown to alter its conventional EPR spectrum at 273 K: additional hyperfine splittings were observed slightly below $g = 2$.[6] The extreme difference between enzyme in fluid solution at 273 K and in frozen solution at 2 K, in addition to the different EPR techniques employed, makes comparison between these two results difficult. Addition of K^+ ion may change the electron spin relaxation rates in fluid solution in a way that has no effect at low temperature. Similar effects of K^+ ion on Mn(II) EPR at ~273 K have been reported in a much earlier study by Reed and Cohn (Reed, G. H.; Cohn, M. *J. Biol. Chem.* **1973**, *248*, 6436−6442) of pyruvate kinase and were attributed to changes in vibrationally induced relaxation mechanisms.

Mechanistically, such an alteration in the protein-derived ligand set would preserve the electrophilicity of the metal center, even after it binds the anionic substrate. Higher electrophilicity is expected to enhance the addition of the anionic nucleophile (GS^-) to the oxirane carbon by increasing the polarization of the C−O bond. The electrophilic assistance provided by the metal could occur by direct interaction of the metal with the oxirane oxygen or via protonation by a metal-bound water molecule (Figure 4).

Conclusions

FosA is of specific interest as an important member of the VOC enzyme superfamily.[4] From a broader chemical/biological point of view, FosA is an unusual metalloenzyme, in that it has a mononuclear Mn(II) center, in contrast to the more numerous dinuclear and tetranuclear Mn enzymes, often with Mn in higher oxidation states.[57] Further, FosA is unique among the relatively few mononuclear Mn enzymes,[7−9] in that the Mn(II) ion is not redox active.

EPR at 35 GHz under adiabatic rapid-passage conditions shows that while FosA-bound Mn(II) (E·Mn^{2+}) still exhibits the typical Mn(II) hyperfine-split sextet in its EPR spectrum, it is notably different from aqueous Mn(II). Quantitative binding of fosfomycin, the enzyme substrate, abolishes this sextet, as also observed by conventional EPR. GS-fosfomycin (the enzyme product) and phosphate ion (an inhibitor) bind with lower association constants, so that conventional EPR only shows the residual E·Mn^{2+}. In contrast, 35-GHz rapid-passage dispersion detection readily reveals the EPR spectra of the ternary complexes of E·Mn^{2+} with substrate/inhibitor/products. This approach, which has not been applied widely by others despite its early success in the detection of the EPR signal of horseradish peroxidase compound I intermediate,[17] can in principle be implemented with any spectrometer that has both dispersion and liquid helium temperature capabilities.

Binding of these small molecules to FosA leads to dramatic changes in the EPR spectra of the enzyme, with a ca. 4-fold increase in both the axial (D) and rhombic (E) zfs parameters of Mn(II). This results leads us to suggest that substrate binding to Mn(II) involves the replacement of two water molecules (by two oxygen donor atoms of substrate/inhibitor/product) *and* loss of an endogenous glutamate ligand. This suggestion is supported by comparison with the crystallographically characterized complex of glyoxalase I (another VOC enzyme) with a transition-state analogue and by comparison with crystallographic and EPR data for MnSOD. This suggestion further provides a rationale for the requirement of potassium ion for enzyme activity. Further investigations involving FosA mutants and pulsed and CW ENDOR are planned to shed light on the FosA mechanism and structure of its complexes.

Acknowledgment. This work was supported by NIH Grant R01 AI42756 (R.N.A.) and training Grants T32 GM08320 (C.L.R.) and T32 ES07028 (B.A.B.) and by NSF Grant MCB9904018 (B.M.H.) and NIH Grant R01 HL13531 (B.M.H.).

(57) Britt, R. D. *Curr. Opin. Struct. Biol.* **1993**, *3*, 774−779.
(58) Misra, S. K.; Sun, J.-S. *Magn. Reson. Rev.* **1991**, *16*, 57−100.
(59) Abragam, A.; Bleaney, B. In *Electron Paramagnetic Resonance of Transition Ions*, 2 ed.; Dover Publications: New York, 1986; pp 436−442.
(60) Sturgeon, B. E.; Ball, J. A.; Randall, D. W.; Britt, R. D. *J. Phys. Chem.* **1994**, *98*, 12871−12883.

We thank Prof. Bruce R. McGarvey, University of Windsor, Canada, for extensive assistance with the derivations given in the Supporting Information.

Supporting Information Available: Derivation of eqs 2a,b and discussion of ligand-field parameters for FosA species and Figures S1−S8 showing additional experimental and simulated EPR spectra and energy level diagrams (PDF). This material is available free of charge via the Internet at http/::pubs.acs.org.

JA012480F